2024 IEEE/RSJ International Conference on Intelligent Robots and Systems (IROS)
October 14-18, 2024. Abu Dhabi, UAE

Kinematic Modeling of Twisted String Actuator Based on Invertible Neural Networks

Zekun Liu[1], Dunwen Wei[1], Tao Gao[1], and Jumin Gong[1]

Abstract— **Twisted String Actuators (TSAs) exhibit several advantages, including lightweight, compact, and having a high power-to-weight ratio. However, current research on kinematic models of TSAs is limited to deriving the relationship between motor input and output through idealized geometric calculations. Therefore, the accuracy of these models does not meet the requirements for practical applications. Previous studies on the kinematic modeling of TSA have not considered the impact of material plastic deformation and stroke times on TSA kinematics. Accumulation of plastic deformation over multiple strokes leads to changes in the output displacement of TSA, significantly affecting the accuracy of the kinematic model. This study aims to address the limitations of previous research by investigating the use of Invertible Neural Networks (INNs) in kinematic modeling of TSAs, taking into account material plastic deformation and stroke times. Through a series of TSA experiments, a kinematic model of TSA was established using an INN that considers stroke times. The INN model proves to be superior in both forward and inverse kinematic modeling by effectively compensating for the effects of plastic deformation during TSA operation. The experimental results demonstrate that the kinematic model established by the proposed INN is more aligned with the actual conditions when compared to traditional kinematic models. This insight can aid in predicting the lifespan of TSA in the future.**

I. Introduction

Twisted String Actuators (TSAs) represent an innovative and groundbreaking type of actuation system that serves the purpose of transferring motor rotation into a linear displacement output. The inherent design of TSAs involves securely fastening one end of strings to the motor, while the other end is firmly attached to the load. Consequently, as the motor initiates its rotational motion, the strings within the TSA start to tighten, leading to an axial contraction phenomenon that ultimately results in a reduction in the overall length of the axial string [1]. Remarkably, one of the key advantages offered by TSAs lies in their ability to achieve high transmission ratios [2], [3]. This impressive feat is accomplished through the strategic utilization of lightweight, low-noise, and cost-effective strings, which serve as a superior alternative to the traditional bulky, high-friction, and expensive gearboxes that are typically employed in other actuation systems.

*This work was supported by the National Natural Science Foundation of China (Grant No. 52275282,51705066), Natural Science Foundation of Sichuan Province (Grant No. 2022NSFSC1960), Fundamental Research Funds for the Central Universities of China (Grant No. ZYGX2021YGCX011), and the Postdoctoral Science Preferential Funding of Zhejiang Province of China (Grant No. ZJ2022123). (Corresponding authors: Dunwen Wei)

[1]Department of Mechanical and Electrical Engineering, University of Electronic Science and Technology of China, Chengdu, 611731, China. weidunwen@uestc.edu.cn

Due to its excellent characteristics, TSA has been widely applied in many robotic systems. For instance, Palli et al. [4] made significant progress by successfully developing a DEXMART Hand that utilizes TSA. They conducted a comprehensive kinematic analysis and proposed a complete control scheme, which greatly enhanced the functionality and versatility of the robotic hand. Building on this foundation, Konda et al. [5] introduced a soft robot bionic hand based on TSA, and they conducted experiments focusing on grasping. Similarly, Li et al. [6] developed a hand rehabilitation glove that relies on TSA, and also introduced a condition detection and multi-functional treatment plan. Tsabedze et al. [7] designed a flexible and lightweight TSA glove, improving the comfort and flexibility of the glove. Additionally, Hosseini et al. [8] created a TSA-based exoskeleton, which has shown promising results in assisting handling activities, paves the way for the development of advanced exoskeleton systems that can assist individuals in performing physically demanding tasks with ease. Furthermore, Lee et al. [9] proposed a human-like spinal assistance robot with a twisted wire drive and a flat back relief mechanism for path planning to effectively reduce spinal wear during motion.

In summary, the studies mentioned above have collectively contributed to the advancements in TSA-based technologies. Through their innovative designs and comprehensive analyses, these researchers have shed light on the potential applications and benefits of TSAs in various domains, including hand prosthetics, soft robotics, rehabilitation, exoskeleton technology, and spine-assist robotics. Their findings and contributions have laid the groundwork for further research and development in this rapidly evolving field.

However, it is important to note that the current accuracy of TSA kinematic models still needs improvement. The current state of research on kinematic models of TSAs still fails to adequately address the requirements of practical applications. This issue arises from the fact that the existing kinematic models were based on geometric expansions and ideal assumptions, resulting in a lack of practical applicability and difficulties in the widespread adoption of traditional TSA kinematic models.

In the aspect of TSA modeling, Godler et al. [10] presented a kinematic model of TSA that is based on the geometric and operational principles of the twisted string. However, this model is flawed as it assumes that there is no contact gap between the strings and that the string radius remains constant. Consequently, there are inherent inaccuracies when this model is applied in practice. Palli et al. [11] examined the impact of force on the kinematic

model of the TSA and explored the overall elongation and reduction in the radius of the string under the influence of force. However, they did not take into consideration the spacing between the two ends of the string in real-world applications. In an effort to address this limitation, Tavakoli et al. [12] considered the impact of spacing on the kinematic model when modeling a TSA with a separator. Nonetheless, their approach was still based on ideal assumptions and overlooked other factors pertinent to actual work. Ryu et al. [13] introduced modifications to the static tension model by incorporating control algorithms that accounted for changes in stiffness and original length. This improved the conditions and tracking performance of the kinematic model in practical applications.

During the operation of TSAs, there are changes in the output displacement due to plastic deformation [5], [14]. With each successive stroke, the string experiences continuous deformation and wear [14]. As a result, the previous kinematic model of TSA gradually becomes inadequate for meeting application requirements. Particularly, when there are slight changes in the initial position, the inverse model of TSA kinematics exhibits significant deviations, posing challenges for practical implementation. While some literature [13], [15] proposes the use of feedback control algorithms to compensate for kinematic errors, the employment of high-precision kinematic models can minimize delays and response times in the control algorithm. This, in turn, enhances the stability of the control algorithm and ensures the accuracy of the solution when the control algorithm is not feasible. Future research should focus on enhancing the precision and reliability of TSA modeling methods to fully exploit its potential and maximize its impact in various applications.

The invertible neural network (INN), first introduced by Dinh et al. [16], achieved highly nonlinear biobjective variation by adopting a novel network structure This design directly maximizes logarithmic likelihood, mapping training data into a distributed decomposition space. This approach addresses the limitations of traditional neural networks, offering a bidirectional solution for input and output. The theory of invertible neural networks has evolved, leading to its application in various domains.

Guan et al. [17] used deep invertible neural networks to conceal multiple images, achieving remarkable improvements in invisibility, security, and recovery. Similarly, Zhou et al. [18] integrated transformers and invertible neural networks into the pan-sharpening field, producing superior visual and quantitative results while maintaining a parsimonious parameter count. Haldemann et al. [19] used conditional invertible neural networks to calculate posterior probabilities for planetary structure parameters, improving the rate of inference for characterizing exoplanets. Huang et al. [20] proposed a wavelet-inspired invertible neural network to enhance the robustness and adaptability of noise reduction neural networks.

Therefore, the focus of this study lies in the utilization of INNs to address the kinematic modeling predicament pertaining to TSAs. INNs possess noteworthy merits when it comes to examining kinematic models of TSAs: their invisibility ensures precision in both forward and inverse tasks, the integration of multi-layer coupling blocks and nonlinear activation functions enables the processing of intricate nonlinear data transformations, the capability of multi-modal modeling can cater to the handling of numerous inputs and outputs, and the adaptability of parameter control renders them suitable for real-world operational conditions.

This article is structured as follows: Section II expounds upon the traditional modeling method of TSAs. The subsequent section III delineates the fundamental principles and specific structures underpinning the utilization of INNs. Following, section IV presents experimental results aimed at substantiating the efficacy of the proposed kinematics model. Finally, section V culminates this article by presenting the conclusion.

II. Modeling method of TSA

This research investigates the model of a TSA with a separator as proposed in the existing literature. The inclusion of a separator between the motor end and the load end impacts on the motion characteristics of the TSA. Firstly, the presence of a separator ensures that the torsion area of the TSA remains within a predetermined range. Additionally, the separator enhances the movement stroke of the TSA and optimizes its utilization. In addition, the separator's structure enables the TSA's transmission ratio to be flexibly adjusted.

Fig. 1 shows the diagram that illustrates the model for the TSA. The twisted string's overall length is denoted as l, while the length of the torsion zone is indicated as d. The distance between the holes in the separator is represented by b, and the radius of the string is accounted for by r. Additionally, the rotation angle of the motor is denoted as θ. Due to the displacement of the end of TSA x, an end load F is experienced. The kinematic model for the TSA model can be easily derived:

$$x = \sqrt{d^2 + (b + \theta r)^2} - d \tag{1}$$

During the practical implementation of the twisted string actuator, it is important to consider the elongation of the twisted string caused by external forces. The length of the twisted string varies as a result of these external forces, and can be described as follows:

$$l = l_0 + \frac{F}{K} \tag{2}$$

In this equation, l_0 represents the original length of the string, and K represents the elastic coefficient of the string. It is assumed that adjacent strings cannot compress each other indefinitely and there are no voids within the string. Therefore, the volume of the string remains constant throughout torsion. Any changes in the length of the string are accompanied by corresponding variations in its radius, which can be expressed as follows:

$$r_v = r\sqrt{\frac{l_0}{l}} \tag{3}$$

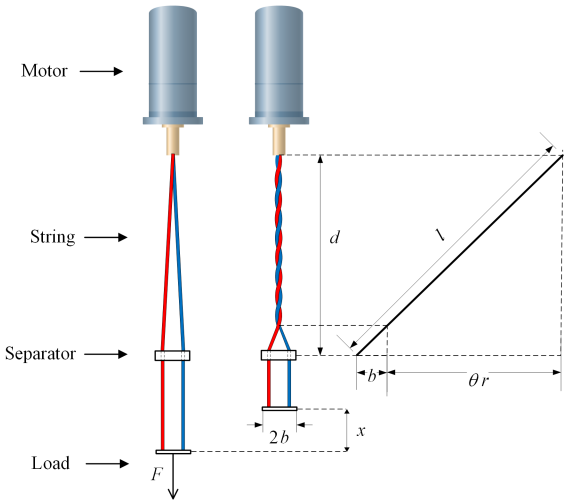

Fig. 1. The schematic diagram of the TSA.

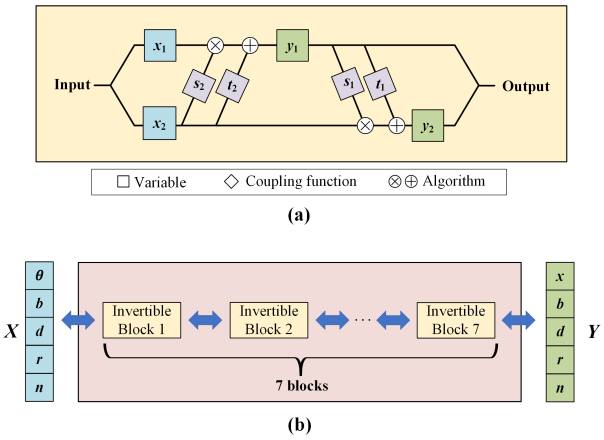

Fig. 2. (a) Invertible block diagram. (b) Invertible neural network structure diagram.

During the torsion process, the variable radius r_v is continuously calculated using Formula 3. Ultimately, the kinematic model of the twisted string actuator can be expressed as follows:

$$x = \sqrt{d^2 + (b + \theta r_v)^2} - d \tag{4}$$

The inverse kinematics model for the twisted string actuator can be derived by inverting the formula mentioned above:

$$\theta = \frac{1}{r_v}\left[\sqrt{(x+d)^2 - d^2} - b\right] \tag{5}$$

Although various studies have made modifications and optimizations, the traditional kinematic model of the TSA still has several significant shortcomings:

(1) The model is based on idealized assumptions that only account for the static deformation of regular strings. These assumptions frequently fail to meet real-world application requirements, resulting in limited accuracy.

(2) The conventional kinematic model does not consider the impact of stroke times. However, the plastic deformation accumulated by multiple strokes will affect the kinematic model of the TSA and, consequently, the accuracy of the model.

(3) The kinematic model used by the TSA contains nonlinearities that cause a significant error in the inverse model when there is a small displacement error in the low-angle regime. The traditional kinematic model is unable to compensate for this error through inverse solution techniques, thereby posing challenges in establishing an accurate inverse kinematic model.

III. Principle of Invertible Neural Networks

Neural networks construct predictive models with the advantageous qualities of adaptability, generality, and flexibility. They have the capability to handle intricate nonlinear relationships, making them a powerful tool for a wide array of prediction and modeling tasks. Typically, traditional neural networks typically consist of weighted connections that link multiple layers of neurons. The activation function of neurons enables neural networks to capture nonlinear relationships between input and output data. However, due to the structural constraints, these networks primarily emphasize forward prediction processes, lacking the ability to perform inverse inferences.

Invertible neural networks have bidirectional mapping capabilities that enable lossless information transfer. Their forward and inverse processes share a common set of parameters, making the model lighter and more tractable during training. Additionally, invertible networks are computationally efficient in both directions, with tractable Jacobian determinants. This feature allows for explicit probability transformations using variable formulas, providing invertible neural networks with benefits in probabilistic modeling and uncertainty estimation.

A. Theory of INN

The invertible neural network consists of a sequential stack of invertible blocks, as visually represented in Fig.2. Within this structure, the output of each individual invertible block serves as the input for the subsequent block, creating a serial dependency between the layers. Each block's output serves as the input for the next block, creating a serial dependency between the layers. To ensure the invertible block's functionality, the number of inputs and outputs must be equal, and the input and output dimensions must be identical. If these conditions are not met, zero padding can be used. The coupling layer receives the input and divides it into two parts using the coupling function. One part is scaled, and the other is shifted based on the output. This process is applied to both parts, and the output is generated through a serial connection. The forward process can be mathematically described as follows:

$$\begin{aligned} y_1 &= x_1 \cdot \exp(s_2(x_2)) + t_2(x_2) \\ y_2 &= x_2 \cdot \exp(s_1(y_2)) + t_2(y_1) \end{aligned} \tag{6}$$

Here, s_i(scale) and t_i(translation) represent arbitrary complex coupling functions, which can be effectively realized by classical neural networks. These networks themselves are irreversible, yet the blocks formed by the nodes are always invertible. The multiplication of the corresponding elements is denoted by $\otimes$, and the addition of the corresponding element is expressed as $\oplus$. In practical applications, an exponential function is used to avoid numerical complications. The coupling layer is entirely invertible, meaning that the input can be reconstructed from the output.

$$\begin{aligned} x_2 &= (y_2 - t_1(y_1)) \cdot \exp(-s_1(y_1)) \\ x_1 &= (y_1 - t_2(x_2)) \cdot \exp(-s_2(x_2)) \end{aligned} \tag{7}$$

Compared to the forward process, the inverse process of the invertible neural network does not introduce any additional computational complexity. Unlike deep Bayesian networks, which can learn any function, the learning in invertible neural networks is based on bidirectional mapping. In general, Bayesian methods inherently lose information during the forward process, leading to fuzziness in the inverse solution. However, the bijective nature of the invertible neural network model structure allows bidirectional operation and training, so that both the forward and inverse processes can be effectively handled during training.

B. Model design

The aim of establishing an invertible neural network is to map the axial displacement of a TSA onto the number of motor turns by designing a TSA with defined parameters, including the length of the torsion zone, the distance between the holes in the separator and the string radius. This objective ensures accurate control and predictability in the system, allowing bidirectional mapping and efficient training of the neural network.

The proposed model design is shown in Fig.2. The invertible neural network model consists of 7 invertible blocks, with mixed layers in between. By disrupting the spatial order of the input data, the expressiveness of the model is enhanced, preventing overfitting, improving the diversity of feature learning, and maintaining the invertibility of the whole network.

Each invertible block contains scale and shift networks, which consist of a fully connected neural network. This neural network consists of three fully connected neural networks, each containing 256 neurons and using a ReLU activation function. The inclusion of nonlinear factors allows the network to accommodate complex nonlinear relationships.

At the forward input end of the model settings, there are five working parameters of the TSA: the rotation angle of the motor, the distance between the holes in the separator, the length of the twisted string, the radius of the twisted string, and the stroke times performed with the twisted string. Similarly, the inverse input end is equipped with five working parameters of the TSA: the axial displacement of the load, the distance between the holes in the separator, the length of the twisted string, the radius of the twisted string, and stroke times performed with the twisted string. As the forward and inverse inputs possess identical dimensions, there is no need to fill the network with zeros.

IV. Experimental Results

A TSA system was implemented to validate the established kinematic model. The system consists of a rotating motor, a separator, and the twisted string. The experimental platform is shown in Fig. 3. The material selected for the twisted string was ultra-high nylon with superior flexibility and strength was chosen to ensure the stability of the wire and prevent any breakage during operation. The entire system is powered by DC power and the system control is accomplished through a MCU. In the data acquisition section, a photoelectric encoded displacement sensor is used as the displacement sensor to detect any changes in displacement at the end of the rope. Finally, the main control board collects data from each sensor and transmits it to the host computer for data analysis.

We performed several experiments on the identical string to observe the changes in its kinematic model resulting from stroke times. We selected experimental data for the strokes n=1,n=3,n=5, n=7, and compared them with the theoretical model, as shown in Fig. 4. It is evident that the kinematic models of the experimental curves have undergone significant changes after multiple strokes compared to the first stroke. The plastic deformation caused by multiple strokes has been documented in the literature [12], [13], but the effect on kinematic models has not been investigated in previous research. However, due to the nonlinear nature of the kinematic model of the TSA, slight error at the low-angle regime will result in a significant error in its inverse kinematics solution, which will deviate significantly from the actual scenario, as shown in Fig. 4. The theoretical model struggles to accurately fit the experimental curve, thus an INN was employed to address the challenge of compensating for the modeling error of the TSA.

The experiment collected a total of 5,000 data points, which were used as a training set for an INN. The network training process of the network included four distinct learning rates, namely 8e-4, 4e-4, 1e-4, and 5e-5. Incorporating different learning rates into the network training process can improve optimization, speed up convergence, and prevent the network from reaching local optimum solutions, thus improving the performance of the model.

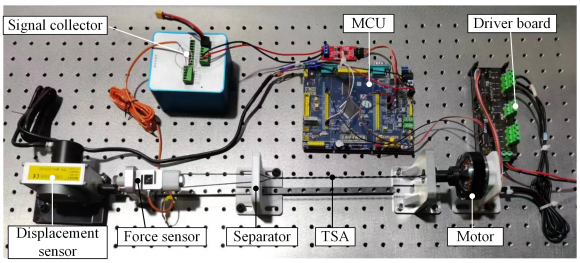

Fig. 3. Experiment platform of TSA

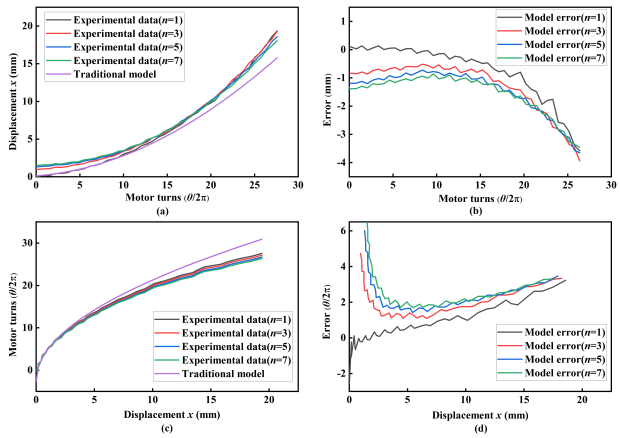

Fig. 4. The effect of stroke times on TSA: (a) Forward kinematics of traditional model. (b) Forward kinematics error. (c) Inverse kinematics of traditional model. (d) Inverse kinematics error.

To verify the compensatory effect of the invertible neural network model on the kinematic model error, we constructed and compared kinematic models corresponding to n=1, n=5, and n=9. The traditional theoretical model served as a benchmark for comparison. Fig. 5 illustrates the differences between the forward and inverse kinematic modeling achieved by the INN and the traditional model. The INN exhibits superior kinematic modeling capabilities compared to the traditional model.

In particular, for n=1, the kinematic model of the TSA has not been affected by the errors caused by the multi-stroke operation. In the low-angle regime, both the traditional kinematic model and the INN show satisfactory modeling results. However, as the angle increases, the modeling error of the traditional model increases progressively, while the INN maintains constant modeling accuracy. Furthermore, when n=5 and n=9, the kinematic model of the TSA changes due to cumulative plastic deformation over multiple strokes. The traditional model fails to account for this factor, leading to significant errors in the low-angle regime. In contrast, the INN compensates for these errors through training with experimental data, resulting in a superior modeling performance.

TABLE I

FORWARD KINEMATICS MODEL ERROR COMPARISON

Model	Stroke times	Average error (mm)	Maximum error (mm)	RMSE (mm)
INN model	n=1	0.180	0.551	0.222
	n=5	0.219	0.544	0.269
	n=9	0.259	0.566	0.311
Traditional model	n=1	1.103	4.382	1.766
	n=5	1.749	4.813	2.094
	n=9	2.101	4.920	2.390

Table I and Table II provide a comparison of the error conditions between the forward and inverse models. The INN model exhibits significantly reduced mean error, maximum error, and RMSE in comparison to traditional theoretical models. In addition, the INN model addresses the problem of large inverse model errors arising from stroke times, thus providing a novel solution for the kinematic modeling of TSAs with significant potential for practical applications.

TABLE II

INVERSE KINEMATICS MODEL ERROR COMPARISON

Model	Stroke times	Average error ($\theta/2\pi$)	Maximum error ($\theta/2\pi$)	RMSE ($\theta/2\pi$)
INN model	n=1	0.584	1.681	0.721
	n=5	0.819	2.234	1.061
	n=9	0.870	2.324	1.112
Traditional model	n=1	1.351	3.861	1.811
	n=5	2.871	6.013	3.140
	n=9	3.239	6.945	3.470

V. CONCLUSION AND FUTURE WORK

In this paper, we have successfully unraveled the profound effect of string plastic deformation on the kinematic model of the TSA during multi-stroke operation. Through the utilization of INN, we have ingeniously developed a forward and inverse bidirectional kinematic model of the TSA. A major concern have addressed in this study is the effect of plastic deformation and stroke times on the model accuracy. By enhancing the precision of the original model, they have effectively mitigated this issue and ensured that the obtained results are reliable and trustworthy. The results of the conducted experiments have unequivocally demonstrated that the newly established kinematic model of the TSA, which incorporates the use of INN, exhibits a considerably higher accuracy when compared to traditional kinematic models.

Not only does this novel approach enhance the accuracy of the kinematic model, but it also plays a pivotal role in diminishing the occurrence of errors in the traditional kinematic model within the initial region of TSA operation. It addresses a key limitation of the traditional models. The INNs for kinematic modeling prove to be a highly effective solution to the challenges posed by plastic deformation and stroke times encountered by traditional models in complex working scenarios.

The experimental results obtained from this study provide compelling evidence that the kinematic model established by the proposed INN is more closely aligned with the actual conditions experienced during TSA operation, in comparison to traditional kinematic models. This finding further underscores the superiority of the newly developed kinematic model and highlights its potential to revolutionize various tasks that require high accuracy and reliability.

Looking towards the future, an interesting avenue for further exploration would be the prediction of the lifespan of TSA after considering the stroke times using INN. This represents an extension of the current research, as it would provide valuable insights into the longevity and durability of TSAs, which is a crucial aspect in many practical applications. By leveraging the power of INN, researchers can

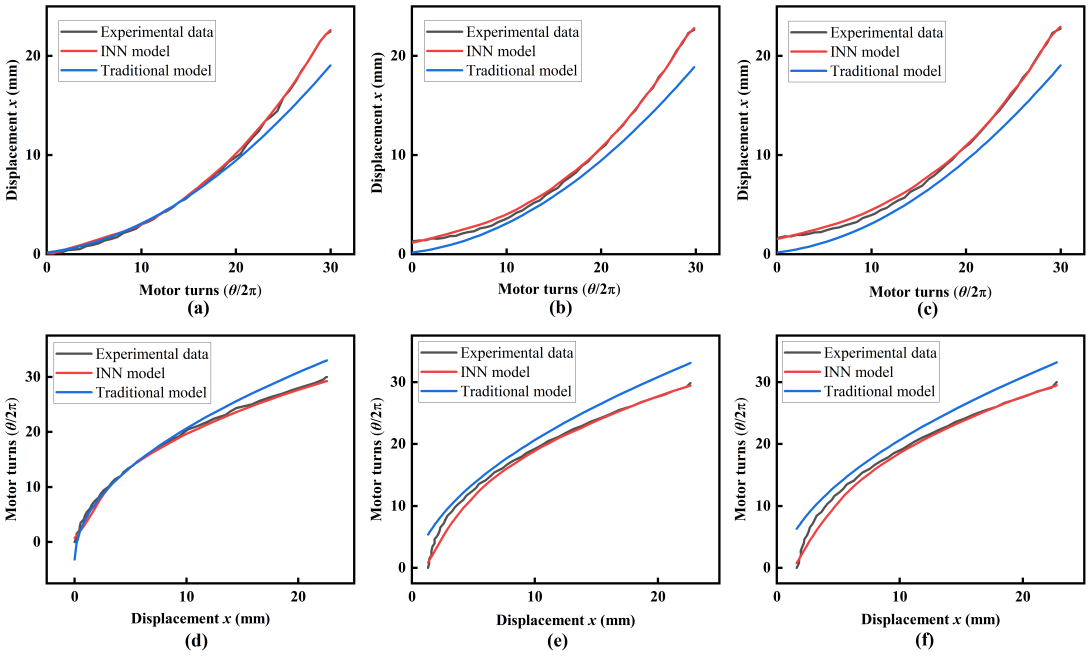

Fig. 5. Results of invertible neural network modeling: (a) Comparison of forward kinematics (n=1). (b) Comparison of forward kinematics (n=5). (c) Comparison of forward kinematics (n=9). (d) Comparison of inverse kinematics (n=1). (e) Comparison of inverse kinematics (n=5). (f) Comparison of inverse kinematics (n=9).

potentially develop predictive models that accurately estimate the lifespan of TSAs, enabling more informed decision-making processes and ultimately leading to improved efficiency and performance in real-world scenarios.

REFERENCES

[1] I. Godler and T. Sonoda, "A five fingered robotic hand prototype by using twist drive," in *ISR 2010 (41st International Symposium on Robotics) and ROBOTIK 2010 (6th German Conference on Robotics)*. VDE, 2010, pp. 1–6.

[2] J. Zhang, J. Sheng, C. T. O'Neill, C. J. Walsh, R. J. Wood, J.-H. Ryu, J. P. Desai, and M. C. Yip, "Robotic artificial muscles: Current progress and future perspectives," *IEEE transactions on robotics*, vol. 35, no. 3, pp. 761–781, 2019.

[3] I. Gaponov, D. Popov, S. J. Lee, and J.-H. Ryu, "Auxilio: A portable cable-driven exosuit for upper extremity assistance," *International Journal of Control, Automation and Systems*, vol. 15, pp. 73–84, 2017.

[4] G. Palli, C. Melchiorri, G. Vassura, U. Scarcia, L. Moriello, G. Berselli, A. Cavallo, G. De Maria, C. Natale, S. Pirozzi, *et al.*, "The dexmart hand: Mechatronic design and experimental evaluation of synergy-based control for human-like grasping," *The International Journal of Robotics Research*, vol. 33, no. 5, pp. 799–824, 2014.

[5] R. Konda, D. Bombara, S. Swanbeck, and J. Zhang, "Anthropomorphic twisted string-actuated soft robotic gripper with tendon-based stiffening," *IEEE Transactions on Robotics*, vol. 39, no. 2, pp. 1178–1195, 2022.

[6] F. Li, J. Chen, Z. Zhou, J. Xie, Z. Gao, Y. Xiao, P. Dai, C. Xu, X. Wang, and Y. Zhou, "Lightweight soft robotic glove with whole-hand finger motion tracking for hand rehabilitation in virtual reality," *Biomimetics*, vol. 8, no. 5, p. 425, 2023.

[7] T. Tsabedze, E. Hartman, and J. Zhang, "A compact, compliant, and biomimetic robotic assistive glove driven by twisted string actuators," *International Journal of Intelligent Robotics and Applications*, vol. 5, pp. 381–394, 2021.

[8] M. Hosseini, R. Meattini, A. San-Millan, G. Palli, C. Melchiorri, and J. Paik, "A semg-driven soft exosuit based on twisted string actuators for elbow assistive applications," *IEEE Robotics and Automation Letters*, vol. 5, no. 3, pp. 4094–4101, 2020.

[9] D. Lee, S. Kim, H.-J. Park, S. Kim, and D. Shin, "A spine assistive robot with a routed twisted string actuator and a flat-back alleviation mechanism for lumbar-degenerative flat back," *IEEE/ASME Transactions on Mechatronics*, vol. 27, no. 6, pp. 5185–5196, 2022.

[10] I. Godler, T. Sonoda, and K. Sakurai, "Modeling and evaluation of a twist drive actuator for soft robotics," *Advanced Robotics*, vol. 26, no. 7, pp. 765–783, 2012.

[11] G. Palli, C. Natale, C. May, C. Melchiorri, and T. Wurtz, "Modeling and control of the twisted string actuation system," *IEEE/ASME Transactions on Mechatronics*, vol. 18, no. 2, pp. 664–673, 2012.

[12] M. Tavakoli, R. Batista, and P. Neto, "A compact two-phase twisted string actuation system: Modeling and validation," *Mechanism and Machine Theory*, vol. 101, pp. 23–35, 2016.

[13] S. Baek and J.-H. Ryu, "Tension control of twisted string actuators in variation of stiffness and original length of strings," *IEEE/ASME Transactions on Mechatronics*, 2023.

[14] R. Konda and J. Zhang, "Hysteresis with lonely stroke in artificial muscles: Characterization, modeling, and inverse compensation," *Mechanical Systems and Signal Processing*, vol. 164, p. 108240, 2022.

[15] D. Bombara, R. Konda, Z. Kibria, and J. Zhang, "Inverse modeling for component selection of twisted string actuators," *IEEE/ASME Transactions on Mechatronics*, vol. 28, no. 2, pp. 1047–1058, 2022.

[16] L. Dinh, D. Krueger, and Y. Bengio, "Nice: Non-linear independent components estimation," *arXiv preprint arXiv:1410.8516*, 2014.

[17] Z. Guan, J. Jing, X. Deng, M. Xu, L. Jiang, Z. Zhang, and Y. Li, "DeepMIH: Deep invertible network for multiple image hiding," *IEEE Transactions on Pattern Analysis and Machine Intelligence*, vol. 45, no. 1, pp. 372–390, 2023.

[18] M. Zhou, X. Fu, J. Huang, F. Zhao, A. Liu, and R. Wang, "Effective pan-sharpening with transformer and invertible neural network," *IEEE Transactions on Geoscience and Remote Sensing*, vol. 60, pp. 1–15, 2022.

[19] J. Haldemann, V. Ksoll, D. Walter, Y. Alibert, R. S. Klessen, W. Benz, U. Koethe, L. Ardizzone, and C. Rother, "Exoplanet characterization using conditional invertible neural networks," *Astronomy & Astrophysics*, vol. 672, p. A180, 2023.

[20] J.-J. Huang and P. L. Dragotti, "WINNet: Wavelet-inspired invertible network for image denoising," *IEEE Transactions on Image Processing*, vol. 31, pp. 4377–4392, 2022.